We are IntechOpen,
the world's leading publisher of
Open Access books
Built by scientists, for scientists

6,900
Open access books available

186,000
International authors and editors

200M
Downloads

Our authors are among the

154
Countries delivered to

TOP 1%
most cited scientists

12.2%
Contributors from top 500 universities

CLARIVATE ANALYTICS
BOOK CITATION INDEX
INDEXED

WEB OF SCIENCE™

Selection of our books indexed in the Book Citation Index
in Web of Science™ Core Collection (BKCI)

Interested in publishing with us?
Contact book.department@intechopen.com

High-Pressure Torsion: Experiments and Modeling

Marina Borodachenkova, Wei Wen and
António Manuel de Bastos Pereira

Additional information is available at the end of the chapter

Abstract

The high-pressure torsion (HPT) process has been the subject of many investigations as a new method of processing for nanostructured materials due to its ability to develop nanostructures with high-angle grain boundaries. This chapter examines the various publications describing the experimental studies of the effect of HPT on the mechanical behaviors and alterations of microstructural features in applications to various pure and alloyed metals. Moreover, an overview of the modeling approaches developed through the last decade, considering the main advantages/limitations, is analyzed.

Keywords: high-pressure torsion, grain refinement, modeling

1. Introduction

The grain size is one of the essential factors controlling the mechanical and physical properties of polycrystals. It is well known that the strength of polycrystalline materials can be improved by reducing the grain size. Materials with fine microstructure usually possess extraordinary properties, including high strength, good toughness, and long fatigue life [1]. For this reason, producing metals with a very small grain size has attracted wide interest recently. To achieve materials with ultrafine-grained (UFG) structures and superior mechanical properties, severe plastic deformation (SPD) has emerged as the fundamental process, as pointed out in review articles by Mazilkin et al. [2] and Zhu et al. [3].

Synthesis of ultrafine-grained (UFG) materials by severe plastic deformation (SPD) refers to various experimental metal forming procedures that may be applied to impose very high strains on materials leading to exceptional grain refinement. One of the most important features of SPD processing is that the shape of the sample is retained by using special tool geometries, which:

1. Prevents the free flow of the material and thereby produces a significant hydrostatic pressure.

2.   Allows imposing strain without any significant change in the overall dimensions of the sample. Therefore, it is possible to repeat SPD process on the sample to achieve extreme large strain.

In the early studies of UFG microstructure formation during SPD, two processing methods have been investigated more intensively: equal channel angular pressing (ECAP) and high-pressure torsion (HPT). These methods have been applied to a wide range of materials: pure metals, alloys, composites, and ceramics. Compared to ECAP, HPT is especially effective to introduce extremely large shear strain which triggers strong grain refinement. In the present chapter, the evolution of the microstructural and mechanical properties during HPT is summarized. Following that, the overview of the modeling approaches applied to predict the microstructure evolution and the stress-strain distribution during HPT is presented.

2. The HPT procedure

A brief introduction of the HPT procedure is presented in this section. More detailed descriptions are available in the literature [2, 3]. The principle of the modern HPT process is illustrated schematically in **Figure 1** [4]. A specimen is held between the plunger and the support and is strained in torsion under the applied pressure (P) in the order of several GPa (1–10 GPa). A lower holder rotates and deforms the specimen by the contact surface friction forces so that deformation proceeds under a quasi-hydrostatic pressure. In practice, there are two main types of HPT processing depending on the shape of the anvils: the unconstrained (**Figure 2a**) and the constrained (**Figure 2b** and **c**) HPT. In unconstrained HPT, samples are placed between two anvils and subjected to HPT processing. In such a case, the sample material is free to flow outward when the
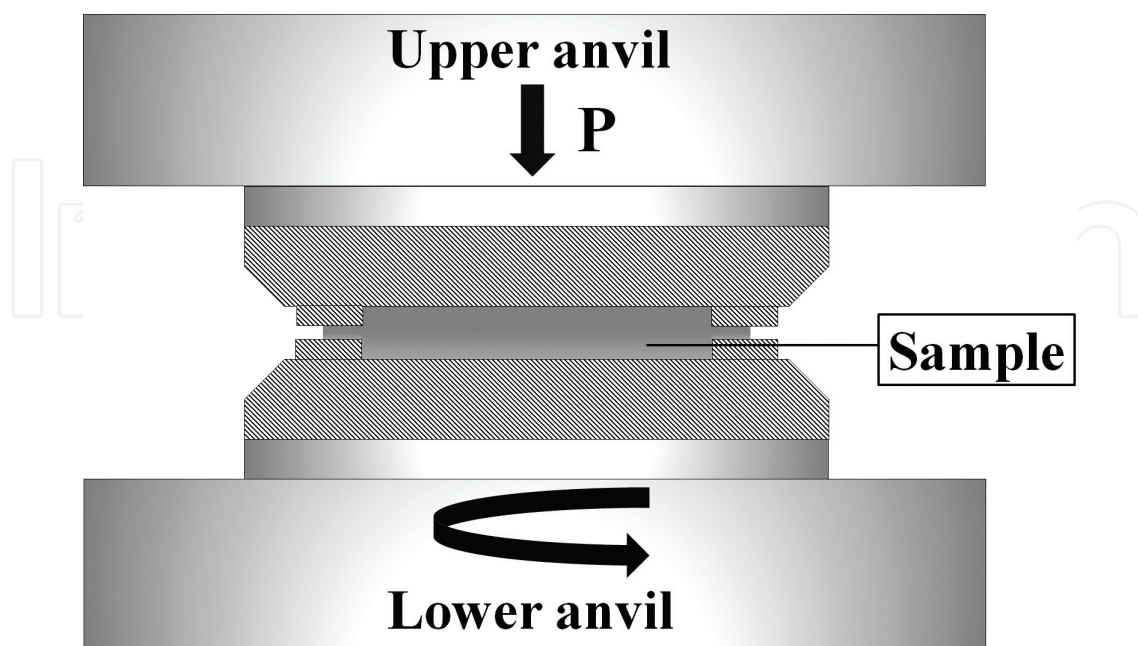

Figure 1. A schematic view of the HPT setup.

high pressure is applied. Samples are thus much thinner after HPT processing [6]. In constrained HPT, samples are placed into the cavity of the lower anvil or both anvils [6], which can prevent material flowing outward. Therefore, the thickness reduction is not evident during HPT. Normally, the constrained HPT is a more common method since this designing is conducted with a more effective back-pressure to the samples [7–9]. However, it is generally difficult to achieve an idealized constrained condition. The experiments are often performed under a quasi-constrained condition where there is at least some limited outward flow between the anvils.

For an infinitely small rotation, $d\theta$, and a displacement, dl, it follows from **Figure 3** that where r is the radius of the disk, the incremental shear strain, $d\gamma$, is given by:

$$d\gamma = \frac{dl}{h} = \frac{rd\theta}{h} \tag{1}$$

where h is the disk thickness.

By further assuming that the thickness of the disk is independent of the rotation angle θ, it follows from formal integration that since $\theta = 2\pi N$, the total shear strain, γ, can be expressed as:
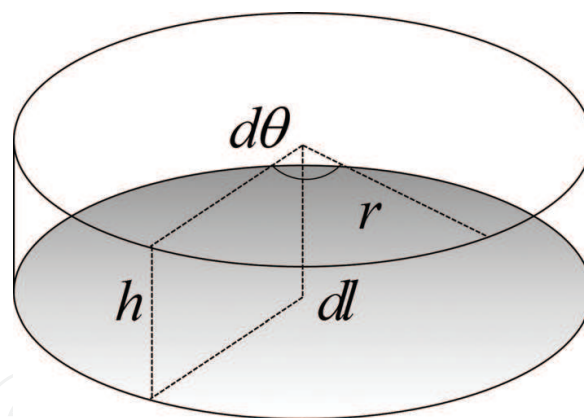
$$\gamma = \frac{2\pi Nr}{h} \tag{2}$$

Figure 2. A schematic view of the sample dimension and the parameters used to estimate the imposed strain in HPT.
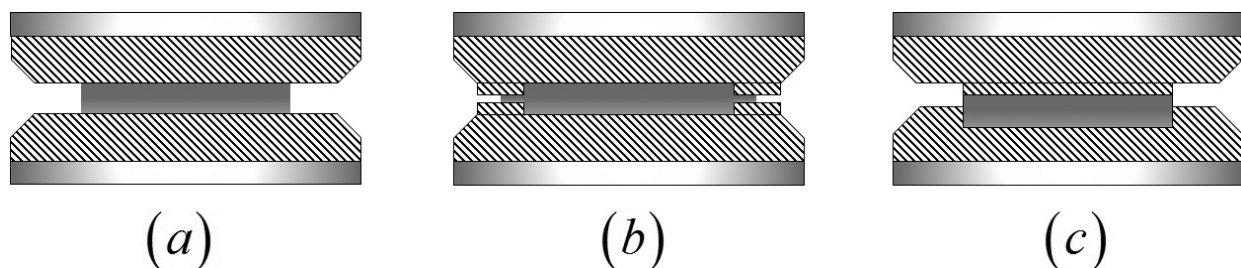

Figure 3. A schematic view of the (a) unconstrained and (b and c) constrained HPT processing conditions.

where N is the number of rotations. The equivalent Von Mises strain is calculated using a commonly used relationship:

$$\varepsilon = \frac{\gamma}{\sqrt{3}} \qquad (3)$$

Theoretically, the imposed strain during HPT is given by Eq. (2). As a result of this expression, the strain is equal to zero at the center of the sample and increases linearly until reaching a maximum near the edges. Thus, the microstructure produced by HPT is heterogeneous. Some authors reported that the microhardness also varies significantly along the radius of disks processed by HPT [10–12].

Nevertheless, it is possible to obtain homogeneous structures along disk diameter by increasing the number of revolutions [4, 13]. For example, in the work of Xu et al. [14], high purity aluminum disks were processed by HPT at room temperature under pressures of 1.25, 2.5, and 6 GPa for 1, 3, and 5 turns. It has been reported that at the early stages of deformation, the hardness at the disk center is higher than that at the edges, and the hardness becomes homogeneous with high level of deformation. This kind of material response has been observed for a material where recovery is rapid, as in the pure aluminum used in this investigation. By contrast, for a material where recovery is slow, the hardness is initially lower in the center, but gradually the microstructure evolves into a homogeneous condition.

In the work of Kawasaki et al. [15], processing by high-pressure torsion has been conducted through 1/4, 1, and 5 turns, and detailed microhardness measurements were recorded on high purity (99.99%) aluminum. The hardness is initially high in the centers of the HPT disks but it decreases with torsional straining to become reasonably homogeneous.

3. Influence of HPT on the mechanical and microstructural properties

The HPT process has been the subject of many investigations due to its ability to develop homogeneous nanostructures with high-angle grain boundaries [16]. The mechanical behavior and microstructural feature evolutions have been extensively studied for a wide range of pure metals and alloys [4, 5, 13, 17–28]. In this section, the overview of the nanosized microstructure formation and the improvements in the mechanical properties during HPT are discussed.

3.1. Grain refinement

A tremendous amount of experimental works has been published on grain refinement by HPT. It has been reported that there is an ultimate minimum grain size that can be achieved by HPT. The results of the grain refinement for various metals and alloys during HPT are summarized in **Table 1**. As it can be seen, refinement ratio varies from 100 to 1800.

Despite the intensive empirical studies on the formation of the ultrafine-grained microstructures, only several studies have attempted to understand the mechanisms of the grain

Metal/alloys	Initial grain size (μm)	Saturated grain size (nm)	Yield stress (MPa)	Pressure (GPa)	Number of rotations	References
Commercial 7075 Al alloy		26	1000	6	10	[29]
Commercial pure Ti	2–10	30	–	5	5	[30]
High purity (99.99%) Ni	100	170	Hv = 3.2 GPa	6	5	[4]
Al-7075 alloy	Extruded lengths up to ~450 μm and widths of ~8 μm	500 (disk center) 250 (disk edge)	Hv~230	6	10	[31]
Cu-0.1 wt% Zr	20	270 (disk center) 230 (disk edge)	–	6	10	[32]
Al-1% Mg	400	230	Hv~110	6	10	[33]
High purity copper	40	200–250	Hv~140	6	10	[34]
Al-5 wt% Fe alloy (metastable supersaturated solid solution)		150		5		[35]
Armco-iron 99.95%	40	100	Hv=4.6 GPa	7	5	[36]
Mg-3%, Al-1% Zn	150–200	150–200	Hv~110	2.5	15	[37]
Pure Al (99.7%)	200–500	800	Hv~600MPa	1	8	[17]
Pure tantalum (99.9%)	60	160	Hv~400 σy = 1300MPa	6	10	[38]
Pure Ti (99.99%)	10	150	Hv~248	2	5	[39]
Pure Zr (99.9%)	30	100	Hv~380 σy = 1150MPa	6	20	[22]
Pure hafnium (99.99%)		180	Hv~360	4	10	[40]

Table 1. The grain refinement during HPT for various metals/alloys.

refinement. Most of the theories are based on the idea that a high dislocation density is introduced in the material due to heavy straining and later the dislocations rearrange into ultrafine grain structures, as illustrated in **Figure 4**. In addition to the dislocation mechanisms for ultrafine-grained microstructure formation, some other mechanisms of the grain refine-ment have been described in the literature. For example, Isik et al. [41] reported that, in the case of Co-Cr-Mo alloy, the deformation-induced phase transformation ($\gamma \rightarrow \varepsilon$) contributes to grain refinement via the formation of ε platelets which subdivide the γ grains. Borodachenkova et al. [42] demonstrated that in Al-Zn alloy, the intense dislocation pinning between Zn precipitates within Al grains produces an effective division of the grains and accelerates the grain refine-ment process. The work of Liu et al. [43] indicated that the microtwins can further promote division and break down the grains into subgrains.
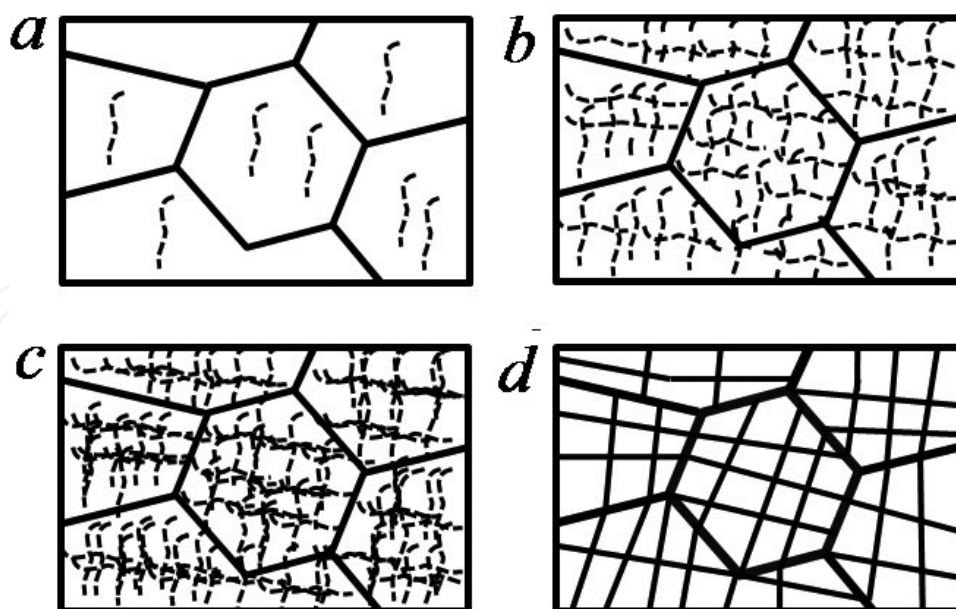
Figure 4. A schematic view of grain refinement during HPT, describing sequentially the processes of (a) the generation/accumulation of dislocations, (b) the formation of subgrain boundaries, (c) the increase in the misorientation angle, and (d) the division of grains into subgrains.

3.2. Improvements in mechanical properties

As it has been widely reported, HPT processing leads to strong grain refinement, and according to the well-known Hall-Petch relation, the material strength is inversely proportional to the grain size. However, the recent works reported that HPT might lead to strain softening and grain refinement simultaneously for pure metals as well as for the alloys. For example, in the work of Ito et al. [44], the purity of Al can evidently influence the material hardness. With increasing Al purity, the grain size dependence of hardness becomes less significant. For ultrahigh pure 6NAl, the hardness variations with respect to the grain size follow an inverse Hall-Petch relationship. The hardness in the HPT-processed state becomes lower, although the grain size (∼20 μm) is smaller than the non-deformed state (larger than 1 mm). The main reason for the observed behavior is that the high-angle grain boundaries act mainly as dislocation sinks (the dislocations moved fast and disappeared in high-angle grain boundaries) in ultrahigh pure Al.

Earlier, Ito and Horita [24] investigated the evolution of the mechanical behavior of pure aluminum during the HPT process. The initial grain size before HPT was 250 μm. After one rotation under hydrostatic pressure of 6 GPa, the average grain size was reduced to approximately several microns. The results show that the hardness of pure Al initially increases with increasing strain and then decreases to a saturation value. Based on the transmission electron microscopy (TEM) observations, the following explanation for the softening behavior has been suggested: in the region where the hardness increases, the dislocation accumulation and the subgrain boundary formation occur. The increase in hardness is attributed to

	High-pressure torsion				Superplasticity			References
Alloy	D (μm)	d_{sat} (nm)	N	P (GPa)	T_t (K)	$\dot{\varepsilon}$ (s^{-1})	L_{max} (%)	
Ti-6Al-7Nb	5	100	5	6	1073K ($\sim$0.58T_m)	2×10^{-3}	930%	[48]
Mg-8%wt Li		500	5	3	298	1×10^{-3}	310	[49]
					323		400	
					343		780	
					423		1010	
					473		1330	
Al-2024	$\sim$33	$\sim$240	5	6	573	2×10^{-2}	520	[50]
						1×10^{-2}	470	
						5×10^{-3}	580	
						2×10^{-3}	460	
						1×10^{-3}	350	
Al-2024	$\sim$33	$\sim$240	5	6	623	2×10^{-2}	410	[50]
						1×10^{-2}	710	
						5×10^{-3}	470	
						2×10^{-3}	640	
						1×10^{-3}	650	
Al-2024	$\sim$33	$\sim$240	5	6	723	2×10^{-2}	220	[50]
						1×10^{-2}	370	
						5×10^{-3}	170	
						2×10^{-3}	380	
						1×10^{-3}	430	
Mg-9% Al-1% Zn	30	1500	10	3	573	1×10^{-1}	410	[51]
						1×10^{-2}	860	
						1×10^{-3}	1050	
						1×10^{-4}	1308	
Al-7075+10% vol Al_2O_3 metal matrix composite	8	300	20	6	623	1×10^{-1}	305	[52]
						1×10^{-2}	595	
						1×10^{-3}	345	
Ti-6Al-4V	9.5	77±15	20	6	673	5×10^{-3}	540	[53]
						1×10^{-3}	540	
						5×10^{-4}	440	
						1×10^{-4}	790	

Table 2. The superplasticity properties after HPT processing.

an increase in dislocation density which causes more chances of the mutual interaction of dislocations within grains and of blocking of dislocation motion by the presence of subgrain boundaries. Later, the dislocation density in the subgrains starts to decrease due to the dislocation annihilation at subgrain boundaries. Meanwhile, this annihilation leads to an increase in the misorientation angles, which will further promote the dislocation absorption at the boundaries [24]. This is the reason why the misorientation increases with straining, and more grains are surrounded by higher-angle boundaries. Finally, hardness saturates at a constant level when the dislocation accumulation is balanced with the dislocation absorption at high-angle boundaries. Pang et al. [45] observed that the HPT processing leads to strain softening for the Cu-Al alloys with SFE higher than 28 mJ/m^2, in which dynamic recovery is more noticeable during plastic deformation. For alloys with the lower SFE of 6 mJ/m^2, the strain softening has been restrained, and strain hardening played a dominant role in the deformation process. Mazilkin et al. [2, 46] demonstrated that the HPT of the Al-Zn (10/20/30%wt) and Al-Mg (5/10%wt) alloys leads to a strong grain refinement (from 15 μm to 370 nm) and decomposition of supersaturated solid solution of Zn and Mg in Al. The decomposition of supersaturated solid solution results in material softening.

3.3. Low-temperature superplasticity

Superplasticity refers to the capability of a polycrystalline metal to perform an elongation of at least 400% in tension load and with an associated value for the strain rate sensitivity. It is well established that the superplastic properties are related to grain refinement of materials [47]. Necessary conditions for the superplasticity are (1) stable fine-grained microstructure (grain size less than 10 μm) and (2) temperature higher than half of the melting temperature. HPT processing is an effective method for grain refinement to the submicrometer or even nanometer level. It is also widely reported that the enhanced superplastic properties have been obtained by HPT processing at relatively low temperatures. The recent results for the superplasticity properties after HPT are summarized in **Table 2** (D—initial grain size, d_{sat}—saturated grain size, N-—number of rotations, P—applied pressure during HPT processing, T_t—testing temperature, T_m—melting point, $\dot{\varepsilon}$—strain rate, and L_{max}—maximum elongation).

4. Modeling

Despite the large quantity of studies performed on HPT, most of them are only dedicated to microstructural and mechanical characterization. Recently, some researchers attempted to develop dislocation-based models to capture microstructural evolutions and the resulting changes in properties under large strain. Some other models, which are rooted in the finite-element method, mainly focus on the description of the stress/strain distribution and evolution along the sample radius, using a more empirical approach to describe the mechanical response without getting into the details of the micromechanisms. This section aims to provide an overview of the modeling approaches developed in the last decade, with a discussion of their main advantages/limitations.

4.1. Microstructure-based approaches

The microstructure-based models, describing the grain refinement due to large strain (particularly under HPT), are usually based on the notion that the dislocation cell walls, which form in the early step of the deformation, transform gradually to high-angle grain boundaries. This type of models are commonly based on the approach of Kocks and Mecking [54], which describes the deformation behaviors of pure metals and alloys via a single internal variable, namely, the total dislocation density ρ_{total}. Estrin [55] proposed a constitutive model to express the hardening behaviors of cell-forming crystalline materials at large strains. A dislocation structure that is developed under torsion deformation can be considered as cellular, with subgrain boundaries containing a high dislocation density separating subgrain interiors where the dislocation density is significantly lower. The volume fraction of the walls f_w is calculated using the following expression:

$$f_w = \frac{2\omega d - \omega^2}{d^2} \tag{4}$$

where ω is the wall thickness and d is the subgrain size, which is proportional to the average dislocation interspacing, $(\propto 1/\sqrt{\rho_{total}})$. The total dislocation density is determined as:

$$\rho_{total} = f_w \rho_w + (1 - f_w)\rho_c \tag{5}$$

where ρ_c is the dislocation density in the cell interior dislocation density, whereas ρ_w is the dislocation density in the cell walls.

The macroscopic stress τ is considered as the sum of the stresses within the walls and cell interiors:

$$\tau = f_w \tau_w + (1 - f_w)\tau_c \tag{6}$$

To validate this model, it has been applied to predict the torsion deformation of pure copper. The predicted hardening curve is compared with experimental results on copper torsion, and a good agreement between theory and experiment is achieved. Since other mechanisms are not accounted for, this model is restricted to the material in which the dislocation hardening is the dominant mechanism.

Zhang et al. [56] has developed a microstructural model that is based on the evolution of geometrically necessary dislocations (GND) and statistically stored dislocations (SSD) that incorporate grain refinement. The total strength of commercially pure aluminum is given as:

$$\sigma_y = \sigma_0 + \Delta\sigma_{gb} + M(\Delta\tau_{dis} + \Delta\tau_{ss}) \tag{7}$$

where σ_0 denotes the strength of annealed aluminum and $\Delta\sigma_{gb}$, $\Delta\tau_{ss}$, and $\Delta\tau_{dis}$ are the contributions due to the grain boundary strengthening, the solid solution hardening, and the dislocations hardening, respectively. The total dislocation density is the sum of the GND and SSD densities. At the center of the disk, the strain should be zero and hence the SSD density (ρ_{SSD})

is expected to be zero. However, the strain gradient is substantial and GNDs will be generated. The density of GNDs depends only on the strain gradient and the magnitude of Burger's vector (*b*) but is irrelevant to the alloying contents. In an idealized cylindrical coordinate, the strain gradient during HPT has only a radial component. Thus, the total amount of GNDs generated per unit volume is given by:

$$\rho_{GND,g} = \frac{1}{b}\frac{d\gamma}{dr} = \frac{2\pi N b}{h} \tag{8}$$

The density of SSDs can be expressed by:

$$\rho_{SSD,g} = \varepsilon\left(\frac{K_A}{M\mu b\alpha}\right)^2 \tag{9}$$

where K_A is an alloy-dependent factor and μ denotes the shear modulus. The grain boundary strengthening is assumed to be inversely proportional to the average grain size:

$$\sigma_{gb} = \mu b\left(\frac{1}{D}\right) \tag{10}$$

The mean grain size, *D*, can be predicted assuming that the average grain boundary misorientation angle, θ, is determined by the dislocation density within the cell wall ρ_{GB}; α is a constant. This approach then provides the following relation:

$$D = 4.365\frac{\theta}{\rho_{GB}b} \tag{11}$$

Model predictions for Al-1050A alloy are given in **Table 3**. The modeling results show an excellent correspondence between measured and predicted average Vickers microhardness (determined as $H_V = \sigma_y/2.9$) at the center of Al-1050A samples processed by m-HPT for different turns. A key element of this model is the assumption that at very high strains, the dislocation density reaches a saturation value. However, the existing models are not capable to connect the flow stress with the observed microstructure evolution.

Turns	$\Delta\tau_{dis}$, MPa	$\Delta\sigma_{gb}$, MPa	σ_y, MPa (predicted)	H_V, MPa (predicted)	H_V, MPa (measured)
0	19	0.4	77	27	30
0.5	28	0.4	101	35	36
1	35	0.4	120	41	41
3	45	4	148	51	49
5	45	7	151	52	52
10	45	10	154	53	54

Table 3. Measured average Vickers microhardness (H_V) in the center of disk compared with model predictions for H_V and the different strengthening components [56].

Recently, Borodachenkova et al. [42] developed a microstructure-based model which allows more detailed analysis of the relative contributions of microstructure hardening mechanisms to the specific softening behavior in Al-30wt% Zn alloys during HPT. The experimental data indicated that the HPT processing leads to a strong softening process at the beginning of plastic deformation before the saturation stage is achieved. The softening is controlled by multiple mechanisms occurring simultaneously during the deformation, which are categorized in Borodachenkova et al. [42] as solid solution decomposition (τ_{ss}), Orowan mechanism (τ_{Orowan}), and dislocation strengthening (τ_{dis}). The total material strength is expressed as:

$$\tau - \tau_{ss} = \tau_{Orowan} + \tau_{dis} \tag{12}$$

Orowan mechanism refers to the strengthening due to the precipitates which act as impenetrable obstacles to the mobile dislocations. When a dislocation is pinned at Zn precipitates, it can still bow out between the precipitates and continue to glide if the driving stress is sufficient. The required stress for the bypass is related to the interspacing (ω) and size of the precipitates (d_p). In Al-Zn alloy, Zn precipitates are formed intensively in the Al grain and grain boundaries at the initial stage of deformation. With increasing strain, the Zn precipitates grow in size due to the diffusion of Zn atoms. Besides, the dislocations pinned at the Zn precipitates tend to transfer gradually into highly misoriented grain boundaries. At large strain, the bulk of Al grains is almost free of precipitates. In this case, theoretically τ_{Orowan} should increase rapidly at the beginning and vanish gradually. To express this process accurately, an empirical factor k_{or} is introduced in the classic Orowan mechanism law [57]:

$$\tau_{Orowan} = k_{or} \frac{0.85 \mu b l n \left(\frac{d_p}{b} \right)}{2\pi \left(\omega - d_p \right)} \tag{13}$$

k_{or} is imposed to be linearly increased to 1 and then reduced to 0 as a function of strain depending on the experimental observations.

The dislocation strengthening term τ_{dis} is expressed using the common Taylor law:

$$\tau_{dis} = \alpha \mu b \sqrt{\rho} \tag{14}$$

where α is the dislocation-dislocation interaction strength parameter. The dislocation density evolution is determined through the Kocks-Mecking-type equation. The dislocation mean free path is a complex matter since it is controlled initially by the precipitates interspacing and, after certain amount of strain, by the refined grain size. Its value is calculated through an empirical law as a function of the strain.

Solute strengthening is related to the interactions between dislocations and solute atoms. When a dislocation is traveling through a randomly distributed solute atom field (commonly known as Cottrell atmosphere), it will suffer a drag force induced by the solute atoms. For the dislocations pinned at obstacles, the diffusion of solute atoms into the dislocation core leads to an increase in the binding energy between the dislocations and their current location. The

effect of solute strengthening depends on the concentration of solute atoms. In Al-Zn, the concentration of Zn atom keeps decreasing due to the precipitation process, which is the main reason for the softening phenomenon. In the work of Borodachenkova et al. [42], the approach of Mecking and Kocks [58] is modified to describe the solute strengthening:

$$\tau_{ss} = k_1 \left(\tau_0 + a_0(c) \left(1 - \left(\frac{kT}{\Delta G} ln \frac{\dot{\gamma}_0}{\dot{\gamma}} \right)^{2/3} \right) \right) \tag{15}$$

where τ_0 denotes the lattice friction, ΔG is the activation energy, and a_0 is the value of thermal stress at 0 K, dependent on the Zn concentration in Al grains (c). a_0 can be written as [59]:

$$a_0 = \tau_p + \frac{3\Lambda}{2b^3} \left(\frac{\sqrt{2}\hat{U}^4}{A\omega_0} \right)^{1/3} \sqrt{c} \tag{16}$$

Here, τ_p is the Peierls stress, $\hat{U}$ the characteristic interaction energy between a single solute and a straight dislocation, ω_0 the characteristic range for the interaction, and A the line tension energy per unit length of dislocation. Comparison of the contributions of the hardening mechanisms is presented in **Figure 5**, which concludes that the shear stress is mostly controlled by the solid solution shear stress. The decomposition of super saturated solid solution plays a dominant role in the material properties of Al-30 wt% Zn alloy.
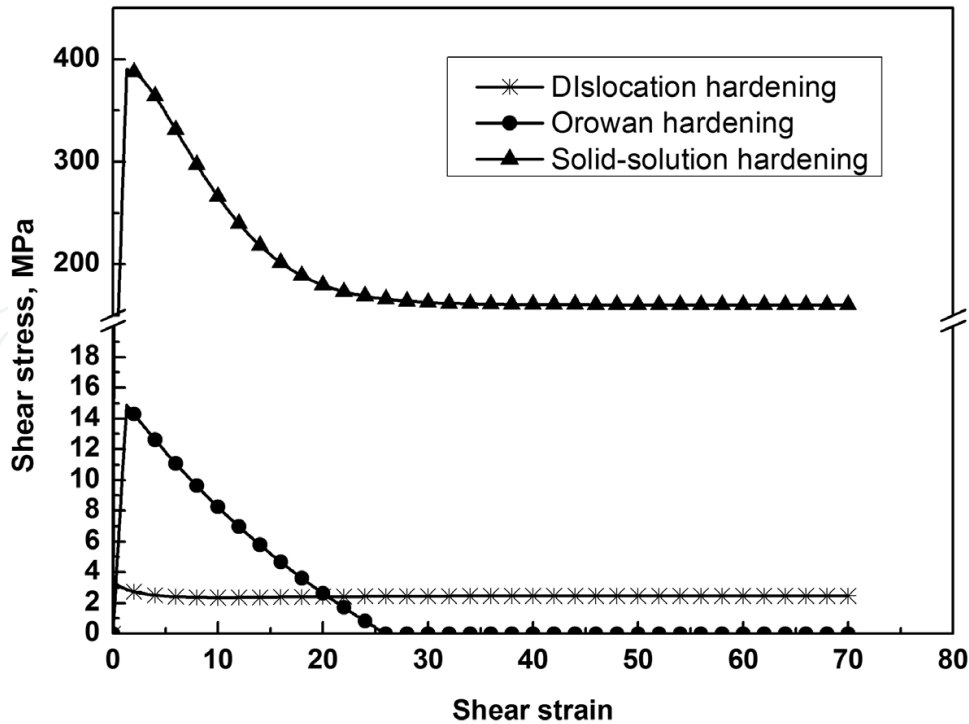

Figure 5. The comparison of the contribution of different hardening mechanisms predicted by the model of Borodachenkova et al. [42].

4.2. Finite-element approaches

The microstructure-based models described in the previous section consider the detailed evolution of the dislocation densities and other mechanisms such as the formation of second-phase precipitates. However, this type of models usually deals with the mechanical behavior at material point level. They cannot describe the heterogeneity of strain/microhardness distributions along the sample radius, which is quite evident during HPT. The finite-element method (FEM) shows an obvious advantage on this matter.

Despite the considerable interest in HPT technique, there are only very limited studies that focus on the heterogeneity of the plastic flow on the sample disk during the processing operation. According to the previous works, the FEM has been an effective tool to study the influence of the disk shape changes as well as the temperature evolutions occurring during HPT processing.

Figueiredo et al. [60] examined the quasi-constrained HPT processing with disks located within depressions on the inner anvil surfaces. The authors conducted the research using DEFORM-3D 10.0 software (Scientific Forming Technologies Corp., Columbus, OH) considering isothermal conditions. The following simulation conditions were taken into account: the applied pressures vary from 0.5 to 2.0 GPa, friction coefficients from 0 to 1 outside of the depressions, and torsional strains up to 1.5 turns. The simulation results show that the mean stresses vary linearly with the distance to the disk center. The authors reported that higher compressive stresses are observed in the disk center and lower stresses at the edge. The compressive mean stresses within the quasi-constrained volume decrease with the increasing extrusion of a ribbon of material between the anvils. The simulations indicate that the distribution of effective strains inside the quasi-constrained volume of the anvils is comparable to the prediction by ideal torsion according to Eqs. (2) and (3). The applied pressure and the friction coefficient outside the quasi-constrained volume play a minor role in the distribution of effective strain.

Later, Figueiredo et al. [61] studied the temperature distribution in quasi-constrained HPT. The calculation results show that the temperature increase within the sample is directly proportional to the material strength and the rotation speed. The temperature increasing rate varies almost linearly with the flow stress of the disk and seems to be independent of the material thermal properties. The study also indicates that a faster rotation speed leads to a higher deformation rate and consequently a higher rate of heating. However, it has been pointed out that the effect of the applied pressure in the HPT on the temperature increase is limited. Figueiredo et al. [61] predicted the evolution of the maximum temperature as a function of time in the iron disk. The results show that the temperature increases from 20 to 54°C during 600 s under 1-GPa pressure. When a much higher pressure of 16 GPa is applied, temperature varies from 20 to 62°C during 600 s. The increase in applied pressure leads to an increase in temperature due to the higher volume of material outflow between the anvils. The predicted temperature increase has been validated by using the experimental measurements of the temperature recorded in the upper anvil during HPT processing of Cu, Mo, and Al. The comparison of the calculated and the measured results depending on the applied pressure and the rotation speed is summarized in **Table 4**.

Material	τ (GPa)	ω (rpm)	P (GPa)	N=1	N=2	N=3	N=4
Cu	0.43	1	2	29.5 (26)	30.7 (28)	33.2 (31)	35.9 (33)
		0.5		25.3 (24)	26.2 (25)	27.9 (26)	29.0 (27)
		0.2		22.6 (21)	23.2 (22)	23.7 (23)	23.7 (23)
Mo	2.22	1	6	66.7 (51)	72.6 (65)	85.4 (87)	98.4 (100)
Al	0.21	5	5	45.7 (28)	47.9 (34)	51.3 (42)	55.5 (47)
		0.2		19.9 (20)	20.3 (20)	20.6 (21)	20.6 (22)

Table 4. Summary of material flow stress (estimated from hardness), the HPT processing parameters, and the temperature predicted at the workpiece (in °C). In parentheses, there are experimental measurements of the temperatures [61].

Song et al. [62] performed a more detailed analysis regarding the influence of the friction on the stress-strain distribution during HPT process. The results demonstrated that friction plays a more important role in the torsion stage than in the compression stage. This chapter also shows (see **Figure 6**) that the effect of the friction coefficient on the effective strain is more significant toward the disk-edge region. The variations of effective strain as a function of the friction coefficient for different locations in the workpiece are also shown in **Figure 6** (right). The authors declared that within the range of friction coefficient from 0.9 to 1.5, the effective strain increases sharply, particularly in the medium and edge areas.

The effect of the friction coefficient on effective strain distribution on the HPT sample is obtained in HPT-FEM simulations after 1 turn under 1-GPa pressure and 1 rpm rotation rate.

4.3. Coupling between micro-macro modeling and FEM

Lee et al. [63] embedded the dislocation density-based constitutive modeling a finite-element code to study the behaviors of pure copper during HPT. The coupling between FEM and microstructure-based constitutive model provides an excellent method for HPT-related
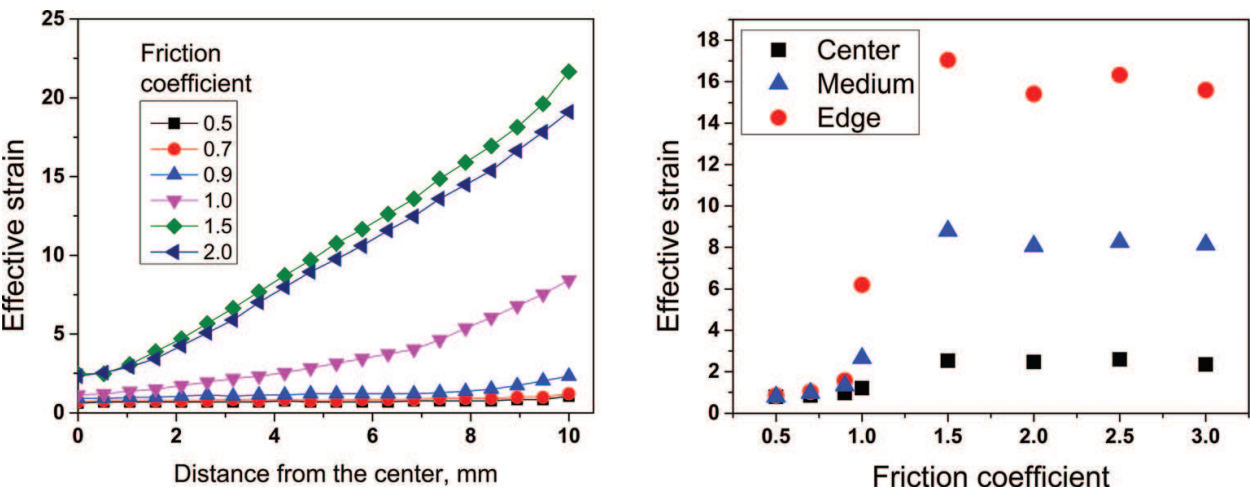

Figure 6. The effect of the friction coefficient on effective strain distribution on the HPT sample, obtained in HPT-FEM simulations after 1 turn under 1-GPa pressure and 1-rpm rotation rate.

predictions, which offers an adequate picture of the variation of the mechanistic parameters, such as stress, strain, and strain rate, as well as the evolution of the microstructural quantities, notably the dislocation density and the average grain size. In Lee et al. [63], the dislocation density evolution is described by the approach of Estrin [55]. The dislocation density-based constitutive model has been embedded in the rigid-plastic FEM package, DEFORM-3D ver. 6.1.

The stress and strain distribution during the HPT process has been analyzed, along with the dislocation density evolution and the concomitant variation of the dislocation cell size. The simulation results were compared with experimentally measured hardness and dislocation density (in the cell interiors and cell walls).The initial dislocation densities in the cell interior are 2.5×10^{13} and 5.0×10^{13} m^{-2}. The gradient of the dislocation density is observed along the sample diameter. After the compression stage, the dislocation densities increase and reach 7.27×10^{14} m^{-2} in the center, 1.0×10^{15} m^{-2} in the middle, and 2.03×10^{15} m^{-2} at the edge region. After one anvil turn, the dislocation densities further increase, and the magnitude is 3.3×10^{15} m^{-2} in the center, 4.70×10^{15} m^{-2} in the middle, and 7.25×10^{15} m^{-2} at the edge region. The difference in the value of the dislocation density between the center and the edge has been explained by the fact that the torsional strain is proportional to the distance from the center as given in Eq. (2). The authors also compared the dislocation density predicted by FEM with the experimental data synchrotron X-ray powder diffraction (XRD) analysis, and a good agreement is achieved.

Author details

Marina Borodachenkova[1]* , Wei Wen[2] and António Manuel de Bastos Pereira[1]

*Address all correspondence to: m.borodachenkova@tue.nl

1 Center for Mechanical Technology and Automation, Mechanical Engineering Department, University of Aveiro, Aveiro, Portugal

2 Materials Science and Technology Division, Los Alamos National Laboratory, Los Alamos, New Mexico, USA

References

[1] Meyers MA, Mishra A, Benson DJ. Mechanical properties of nanocrystalline materials. Progress in Materials Science. 2006;**51**:427–556

[2] Mazilkin AA, Straumal BB, Rabkin E, Baretzky B, Enders S, Protasova SG, Kogtenkova OA, Valiev RZ. Softening of nanostructured Al-Zn and Al-Mg alloys after severe plastic deformation. Acta Materialia. 2006;**54**:3933–3939

[3] Zhu YT, Lowe TC, Langdon TG. Performance and applications of nanostructured materials produced by severe plastic deformation. Scripta Materialia. 2004;**51**:825–830

[4] Zhilyaev AP, Lee S, Nurislamova GV, Valiev RZ, Langdon TG. Microhardness and microstructural evolution in pure nickel during high-pressure torsion. Scripta Materialia. 2001;**44**:2753–2758

[5] Islamgaliev RK, Chmelik F, Kuzel R. Thermal structure changes in copper and nickel processed by severe plastic deformation. Materials Science and Engineering: A. 1997;**234-236**:335–338

[6] Zhilyaev AP, McNelley TR, Langdon TG. Evolution of microstructure and microtexture in fcc metals during high-pressure torsion. Journal of Materials Science. 2007;**42**:1517–1528

[7] Figueiredo RB, Langdon TG. Using severe plastic deformation for the processing of advanced engineering materials. Materials Transactions. 2009;**50**:1613–1619

[8] Krystian M, Setman D, Mingler B, Krexner G, Zehetbauer MJ. Formation of superabundant vacancies in nano-Pd-H generated by high-pressure torsion. Scripta Materialia. 2010;**62**:49–52

[9] Zhang J, Gao N, Starink MJ. Al-Mg-Cu based alloys and pure Al processed by high pressure torsion: The influence of alloying additions on strengthening. Materials Science and Engineering: A. 2010;**527**:3472–3479

[10] Jiang H, Zhu YT, Butt DP, Alexandrov IV, Lowe TC. Microstructural evolution, microhardness and thermal stability of HPT-processed Cu. Materials Science and Engineering: A. 2000;**290**:128–138

[11] Vorhauer A, Pippan R. On the homogeneity of deformation by high pressure torsion. Scripta Materialia. 2004;**51**:921–925

[12] Yang Z, Welzel U. Microstructure-microhardness relation of nanostructured Ni produced by high-pressure torsion. Materials Letters. 2005;**59**:3406–3409

[13] Zhilyaev AP, Nurislamova GV, Kim BK, Baró MD, Szpunar JA, Langdon TG. Experimental parameters influencing grain refinement and microstructural evolution during high-pressure torsion. Acta Materialia. 2003;**51**:753–765

[14] Xu C, Horita Z, Langdon TG. The evolution of homogeneity in processing by high-pressure torsion. Acta Materialia. 2007;**55**:203–212

[15] Kawasaki M, Alhajeri SN, Xu C, Langdon TG. The development of hardness homogeneity in pure aluminum and aluminum alloy disks processed by high-pressure torsion. Materials Science and Engineering: A. 2011;**529**:345–351

[16] An XH, Wu SD, Zhang ZF, Figueiredo RB, Gao N, Langdon TG. Evolution of microstructural homogeneity in copper processed by high-pressure torsion. Scripta Materialia. 2010;**63**:560–563

[17] Zhilyaev AP, Oh-ishi K, Langdon TG, McNelley TR. Microstructural evolution in commercial purity aluminum during high-pressure torsion. Materials Science and Engineering: A. 2005;**410-411**:277–280

[18] Mishra RS, Valiev RZ, McFadden SX, Mukherjee AK. Tensile superplasticity in a nano-crystalline nickel aluminide. Materials Science and Engineering: A. 1998;**252**:174–178

[19] Sakai G, Horita Z, Langdon TG. Grain refinement and superplasticity in an aluminum alloy processed by high-pressure torsion. Materials Science and Engineering: A. 2005;**393**:344–351

[20] Lugo N, Llorca N, Cabrera JM, Horita Z. Microstructures and mechanical properties of pure copper deformed severely by equal-channel angular pressing and high pressure torsion. Materials Science and Engineering: A. 2008;**477**:366–371

[21] Edalati K, Fujioka T, Horita Z. Microstructure and mechanical properties of pure Cu processed by high-pressure torsion. Materials Science and Engineering: A. 2008;**497**:168–173

[22] Edalati K, Horita Z, Yagi S, Matsubara E. Allotropic phase transformation of pure zirconium by high-pressure torsion. Materials Science and Engineering: A. 2009;**523**:277–281

[23] Todaka Y, Sasaki J, Moto T, Umemoto M. Bulk submicrocrystalline ω-Ti produced by high-pressure torsion straining. Scripta Materialia. 2008;**59**:615–618

[24] Ito Y, Horita Z. Microstructural evolution in pure aluminum processed by high-pressure torsion. Materials Science and Engineering: A. 2009;**503**:32–36

[25] Edalati K, Horita Z. Significance of homologous temperature in softening behavior and grain size of pure metals processed by high-pressure torsion. Materials Science and Engineering: A. 2011;**528**:7514–7523

[26] Edalati K, Yamamoto A, Horita Z, Ishihara T. High-pressure torsion of pure magnesium: Evolution of mechanical properties, microstructures and hydrogen storage capacity with equivalent strain. Scripta Materialia. 2011;**64**:880–883

[27] Ni S, Wang YB, Liao XZ, Alhajeri SN, Li HQ, Zhao YH, Lavernia EJ, Ringer SP, Langdon TG, Zhu YT. Strain hardening and softening in a nanocrystalline Ni–Fe alloy induced by severe plastic deformation. Strain. 2011;**528**:3398–3403

[28] Srinivasarao B, Zhilyaev AP, Langdon TG, Pérez-Prado MT. On the relation between the microstructure and the mechanical behavior of pure Zn processed by high pressure torsion. Materials Science and Engineering: A. 2013;**562**:196–202

[29] Liddicoat PV, Liao X-Z, Zhao Y, Zhu Y, Murashkin MY, Lavernia EJ, Valiev RZ, Ringer SP. Nanostructural hierarchy increases the strength of aluminium alloys. Nature Communications. 2010;**1**:63

[30] Dutkiewicz J, Kuśnierz J, Maziarz W, Lejkowska M, Garbacz H, Lewandowska M, Dobromyslov AV, Kurzydłowski KJ. Microstructure and mechanical properties of nanocrystalline titanium and Ti-Ta-Nb alloy manufactured using various deformation methods. Physica Status Solidi: Applications and Materials Science. 2005;**202**:2309–2320

[31] Sabbaghianrad S, Kawasaki M, Langdon TG. Microstructural evolution and the mechanical properties of an aluminum alloy processed by high-pressure torsion. Journal of Materials Science. 2012;**47**:7789–7795

[32] Sabbaghianrad S., Wongsa-Ngam J, Kawasaki M, Langdon TG. An examination of the saturation microstructures achieved in ultrafine-grained metals processed by high-pressure torsion. Journal of Materials Research and Technology. 2014;**3**:319–326

[33] Huang Y, Xu J, Langdon TG. Developing ultrafine-grained materials with high strength and good ductility for micro-forming applications. MATEC Web of Conferences. 2015;21:7002

[34] Xu J, Li J, Wang CT, Shan D, Guo B, Langdon TG. Evidence for an early softening behavior in pure copper processed by high-pressure torsion. Journal of Materials Science. 2016;**51**:1923–1930

[35] Stolyarov VV, Soshnikova EP, Brodova IG, Bashlykov DV, Kil'mametov AR. The aging effect in an ultrafine-grained Al-5% Fe alloy produced by severe plastic deformation. Physics of Metals and Metallography. 2002;**93**:567–574

[36] Valiev RZ, Ivanisenko YV, Rauch EF, Baudelet B. Structure and deformaton behaviour of Armco iron subjected to severe plastic deformation. Acta Materialia. 1996;**44**:4705–4712

[37] Stráská J, Janeček M, Gubicza J, Krajňák T, Yoon EY, Kim HS. Evolution of microstructure and hardness in AZ31 alloy processed by high pressure torsion. Materials Science and Engineering: A. 2015;**625**:98–106

[38] Maury N, Zhang NX, Huang Y, Zhilyaev AP, Langdon TG. A critical examination of pure tantalum processed by high-pressure torsion. Materials Science and Engineering: A. 2015;**638**:174–182

[39] Podolskiy AV, Mangler C, Schafler E, Tabachnikova ED, Zehetbauer MJ. Microstructure and mechanical properties of high purity nanostructured titanium processed by high pressure torsion at temperatures 300 and 77 K. Journal of Materials Science. 2013;**48**:4689–4697

[40] Edalati K, Horita Z, Mine Y. High-pressure torsion of hafnium. Materials Science and Engineering: A. 2010;**527**;2136–2141

[41] Isik M, Niinomi M, Liu H, Cho K, Nakai M, Horita Z, Sato S, Narushima T, Yilmazer H, Nagasako M. Grain refinement mechanism and evolution of dislocation structure of Co-Cr-Mo alloy subjected to high-pressure torsion. Materials Transactions. 2016;**57**:1109–1118

[42] Borodachenkova M, Barlat F, Wen W, Bastos A, Grácio JJ. A microstructure-based model for describing the material properties of Al-Zn alloys during high pressure torsion. International Journal of Plasticity. 2015;**68**:150–163

[43] Liu M, Roven HJ, Liu X, Murashkin M, Valiev RZ, Ungár T, Balogh L. Grain refinement in nanostructured Al-Mg alloys subjected to high pressure torsion. Journal of Materials Science. 2010;**45**:4659–4664

[44] Ito Y, Edalati K, Horita Z. High-pressure torsion of aluminum with ultrahigh purity (99.9999%) and occurrence of inverse Hall-Petch relationship. Materials Science and Engineering: A. 2017;**679**:428–434

[45] Pang Y, Li P, Kim HS, Gong Y, Shen Y, Sun L, Zhu X. Strain softening induced by high pressure torsion in copper alloys. Materials Transactions. 2015;**56**:1658–1663

[46] Mazilkin AA, Straumal BB, Borodachenkova MV, Valiev RZ, Kogtenkova OA, Baretzky B. Gradual softening of Al-Zn alloys during high-pressure torsion. Materials Letters. 2012;**84**:63–65

[47] Kawasaki M, Langdon TG. Review: Achieving superplasticity in metals processed by high-pressure torsion. Journal of Materials Science. 2014;**49**:6487–6496

[48] Ashida M, Chen P, Doi H, Tsutsumi Y, Hanawa T, Horita Z. Superplasticity in the Ti-6Al-7Nb alloy processed by high-pressure torsion. Materials Science and Engineering: A. 2015;**640**:449–453

[49] Matsunoshita H, Edalati K, Furui M, Horita Z. Ultrafine-grained magnesium-lithium alloy processed by high-pressure torsion: Low-temperature superplasticity and potential for hydroforming. Materials Science & Engineering A. 2015;**640**:443–448

[50] Alhamidi A, Horita Z. Grain refinement and high strain rate superplasticity in aluminium 2024 alloy processed by high-pressure torsion. Materials Science and Engineering: A. 2015;**622**:139–145

[51] Al-Zubaydi ASJ, Zhilyaev AP, Wang SC, Reed PAS. Superplastic behaviour of AZ91 magnesium alloy processed by high-pressure torsion. Materials Science and Engineering: A. 2015;**637**:1–11

[52] Sabbaghianrad S, Langdon TG. Developing superplasticity in an aluminum matrix composite processed by high-pressure torsion. Materials Science and Engineering: A. 2016;**655**:36–43

[53] Fu J, Ding H, Huang Y, Pereira PHR, Zhang W, Langdon TG. Grain refining of a Ti-6Al-4V alloy by high-pressure torsion and low temperature superplasticity. Materials Letters. 2015;**5**:281–286

[54] Kocks UF, Mecking H. Physics and phenomenology of strain hardening: The FCC case. Progress in Materials Science. 2003;**48**:171–273

[55] Estrin Y. Dislocation theory based constitutive modelling: Foundations and applications. Journal of Materials Processing Technology. 1998;**80-81**:33–39

[56] Zhang J, Gao N, Starink MJ. Microstructure development and hardening during high pressure torsion of commercially pure aluminium: Strain reversal experiments and a dislocation based model. Materials Science and Engineering: A. 2011;**528**:2581–2591

[57] Kocks UF. A statistical theory of flow stress and work-hardening. Philosophical Magazine. 1966;**13**:541–566

[58] Mecking H, Kocks UF. Kinetics of flow and strain-hardening. Acta Metallurgica. 1981;**29**:1865–1875

[59] Olmsted DL, Hector LG, Curtin WA. Molecular dynamics study of solute strengthening in Al/Mg alloys. Journal of the Mechanics and Physics of Solids. 2006;**54**:1763–1788

[60] Figueiredo RB, Cetlin PR, Langdon TG. Using finite element modeling to examine the flow processes in quasi-constrained high-pressure torsion. Materials Science and Engineering: A. 2011;**528**:8198–8204

[61] Figueiredo RB, Pereira PHR, Aguilar MTP, Cetlin PR, Langdon TG. Using finite element modeling to examine the temperature distribution in quasi-constrained high-pressure torsion. Acta Materialia. 2012;**60**:3190–3198

[62] Song Y, Wang W, Gao D, Yoon EY, Lee DJ, Kim HS. Finite element analysis of the effect of friction in high pressure torsion. Metals and Materials International. 2014;**20**:445–450

[63] Lee DJ, Yoon EY, Ahn D-H, Park BH, Park HW, Park LJ, Estrin Y, Kim HS. Dislocation density-based finite element analysis of large strain deformation behavior of copper under high-pressure torsion. Acta Materialia. 2014;**76**:281–293